

# Particle localization on helical nanoribbons: Quantum analog of the Coriolis effect

Radha Balakrishnan<sup>(1)</sup>, Rossen Dandoloff<sup>(2)</sup>, Victor Atanasov<sup>(2)</sup> and Avadh Saxena<sup>(3)</sup>

<sup>(1)</sup>The Institute of Mathematical Sciences, Chennai 600 113, India

<sup>(2)</sup>Department of Condensed Matter Physics and Microelectronics, Faculty of Physics, Sofia University, 5  
Blvd. J. Bourchier, 1164 Sofia, Bulgaria

<sup>(3)</sup>Theoretical Division and Center for Nonlinear Studies, Los Alamos National Laboratory, Los Alamos,  
New Mexico 87545, USA

**Abstract:** We derive the Schrödinger equation for a particle confined to the surface of a normal and a binormal helical nanoribbon, obtain the quantum potentials induced by their respective curved surface geometries, and study the localized states of the particle for each ribbon. When the particle momentum satisfies a certain geometric condition, the particle localizes near the inner edge for a normal ribbon, and on the central helix for a binormal ribbon. This result suggests the presence of a pseudo-force that pushes the particle transversely along the width of the ribbon. We show that this phenomenon can be interpreted as a quantum analog of the Coriolis effect, which causes a transverse deflection of a classical particle moving in a rotating frame. We invoke Ehrenfest's theorem applicable to localized states and identify the quantized angular velocities of the rotating frames for the two ribbons. If the particle is an electron, its localization at a specific width gives rise to a Hall-like voltage difference across the ribbon's width. However, unlike in the Hall effect, its origin is not an applied magnetic field, but the ribbon's curved surface geometry. When a normal helical ribbon is mechanically flipped to a binormal configuration in a periodic fashion, it results in a periodic electron transport from the inner edge to the center, giving rise to a quantum AC voltage. This can be used for designing nanoscale electromechanical devices. Quantum transport on a helical nanoribbon can be controlled by tuning the bends and twists of its surface, suggesting diverse applications in biopolymers and nanotechnology.

# 1 Introduction

Helical nanostructures appear in various contexts in nature. DNA [1], alpha-helices as well as beta-sheets in proteins [2] are some well known examples in biology. In addition, with the advent of nanotechnology, the fabrication of helical structures with specific geometries has been attracting the attention of materials scientists in order to create devices such as miniature electromechanical sensors [3]. Helically shaped chiral organic molecules called helicenes [4] have been used in designing chemical sensors and in optical applications.

In this paper, we focus on helical ribbons. Such ribbons have been fabricated using a variety of materials such as silicon carbide, silicon oxide, zinc oxide, carbon (graphene nanoribbons), molybdenum disulphide, tungsten disulphide, etc. [5, 6, 7, 8]. In general, helical ribbons can be broadly classified into two types, called *normal* and *binormal* helical ribbons [9, 10, 11]. These differ in their surface geometries. Interestingly, using Kirchhoff's model for helical strips, it has been shown [9] that only these two types of helical strips represent consistent and dynamically stable configurations.

To understand the transport properties of a particle on a helical ribbon of *nanodimensions*, it is imperative to study its *quantum* behavior on the curved surface of the ribbon. A formulation for studying the quantum mechanics of a particle confined to any *general* curved surface has been given by da Costa [12]. It leads to a geometric potential of the form  $V = \frac{\hbar^2}{2m}(M^2 - K)$  in the Schrödinger equation for a particle of mass  $m$ . Here,  $M$  and  $K$  represent, respectively, the mean and Gaussian curvatures [13] of the surface concerned. These arise essentially due to the embedding of the 2D curved surface in 3D space. In this paper, we apply this formulation to the surfaces of normal and binormal helical nanoribbons, with a view to predict their respective surface curvature effects on quantum particle transport.

Our methodology is as follows: As is well known, a curve in 3D space can be represented in terms of its curvature and torsion, by using the Frenet-Serret equations [13]. These describe the rotation of the frame made up of the orthogonal unit triad of vectors consisting of its local tangent  $\mathbf{t}$ , the normal  $\mathbf{n}$  and the binormal  $\mathbf{b}$  vectors, as one moves along the curve. We begin by constructing the surfaces of normal and binormal helical ribbons, using a central circular helix as the base curve, with their widths along  $\mathbf{n}$  and  $\mathbf{b}$ , respectively. We then determine the mean curvature and the Gaussian curvature [13] for

the curved surfaces of the two ribbons. We write down the Schrödinger equation for a particle on these curved surfaces by using the Laplace-Beltrami operator, and obtain the curved-geometry induced potential experienced by the quantum particle using da Costa's formulation [12]. This potential, which is purely quantum mechanical in origin, consists of a contribution from the intrinsic (metric) of the surface, as well as a contribution arising from the extrinsic term that depends on the mean and Gaussian curvatures. We then analyze the expressions obtained for the effective quantum geometric potential for the two helical ribbons. It is seen to depend on both the curvature and the torsion (i.e., twist) of the basic helix used to construct the ribbon surfaces.

We obtain several interesting results. When the quantum particle momentum along the longitudinal helical direction on the ribbon satisfies a certain geometric condition, the induced quantum geometric potential supports localized states in the transverse direction, i.e., on the width of the ribbon. We show that the particle gets localized near the inner edge for the normal helical ribbon, and on the central helix for the binormal helical ribbon. This result suggests the presence of a pseudo-force which deflects the particle transversely along the width of the ribbon, to cause its localization at distinct width values on the two ribbons.

If the particles are electrons, the above localization effect leads to the accumulation of a negative charge near the inner edge of the normal helical ribbon, and on the central helix for the binormal ribbon. This gives rise to a corresponding transverse quantum voltage on the ribbon. However, this effect is unlike the well known Hall effect which arises only in the presence of a magnetic field [14, 15]. For the two types of helical ribbons, it is their distinct curved surface geometries that give rise to the two types of Hall-like voltages. Similarity with the Hall effect suggests the presence of a fictitious 'magnetic field' on the ribbon whose origin is in the curved geometry of the ribbon. Note that the Hall effect without a magnetic field in condensed matter is known as the anomalous Hall effect (AHE) [16] and its quantum analog as the quantum anomalous Hall effect (QAHE) [17].

Interestingly, it has been noted recently that by twisting layers of tungsten disulfide ( $\text{WS}_2$ ) to form a 3D spiral, one generates an electron-path deflecting effect. It has been termed 'twistronic Hall effect' [18], since it is a Hall-like effect observed in the absence of a magnetic field. Moreover, this effect is seen to

mirror [19] the Coriolis effect [20] that is associated with the deflection of a moving particle observed in rotating (noninertial) systems. We parenthetically remark that quantum Coriolis force has been previously mentioned in the context of non-Hermitian Hamiltonians [21].

This motivates us to ask whether the surface geometry induced pseudo-force we had alluded to earlier, which causes the quantum particle (including an electron) to localize along the ribbon width, can be interpreted as a quantum analog of the Coriolis force which causes a transverse deflection of a classical particle moving in a rotating frame. We answer this question in the affirmative. By invoking Ehrenfest's theorem [22] applicable to localized states, we present a detailed analysis to find the expressions for the quantized angular velocities of the rotating frames for the two ribbons, and corroborate this interpretation.

We discuss the case when the length  $L$  of the central helix on the helical ribbon is composed of  $q$  full  $2\pi$  turns. We show that the quantized values of the momentum  $k$  are given in terms of two integers  $n$  and  $q$ , i.e.,  $k = k_{n,q} = (n/2q)\sqrt{(k_0^2 + \tau_0^2)}$ ,  $n = 1, 2, 3, \dots$ . Here  $k_0$  and  $\tau_0$  are the curvature and torsion of the helix, to be defined in the next section. We find that the condition for the existence of localized states is given by  $1 \leq n^2 \leq q^2$ . This gives the interesting result that for such states, the quantum number  $n$  gets restricted by the number  $q$  representing full turns of the helix.

Various applications of our results on localized states can be envisaged. For example, mechanically flipping a binormal helical ribbon to a normal helical configuration in a periodic fashion leads to periodic electron transport between the central helix and the inner edge, resulting in an AC voltage. This may be useful in designing electromechanical sensors [3]. If the nanoribbons are elastic, then depending on the surface elastic energy and the electronic energy, injection of electrons on a binormal helical ribbon can twist it into a normal helical ribbon configuration or vice versa. This phenomenon, which could possibly arise spontaneously in some environments, may be important in biopolymers. Our results demonstrate explicitly that the transport of a quantum particle on a helical nanoribbon can be controlled by tuning the bends and twists of the ribbon surface, suggesting potential applications in nanotechnology.

## 2 Construction of normal and binormal helical ribbons

A circular helix is represented in terms of its arc length  $s$  as  $\mathbf{R}(s) = [R_0 \cos \alpha s, R_0 \sin \alpha s, (P_0/2\pi)\alpha s]$ , where  $R_0$  is the radius of the helix,  $P_0$  is its pitch and  $\alpha = 2\pi/\sqrt{4\pi^2 R_0^2 + P_0^2}$ . Thus,  $\mathbf{t}(s) = d\mathbf{R}/ds = \alpha[-R_0 \sin \alpha s, R_0 \cos \alpha s, P_0/2\pi]$  is the *unit tangent vector* on the helix. The *unit normal vector* is defined as  $\mathbf{n}(s) = \mathbf{t}_s/|\mathbf{t}_s|$ , and the *unit binormal vector* as  $\mathbf{b}(s) = [\mathbf{t}(s) \times \mathbf{n}(s)]$ . These lie on a plane perpendicular to the tangent  $\mathbf{t}(s)$ . The orthonormal unit vector triad  $[\mathbf{t}, \mathbf{n}, \mathbf{b}]$  for a *general* curve satisfies the well known Frenet-Serret equations [13]

$$\mathbf{t}_s = \kappa \mathbf{n} ; \quad \mathbf{n}_s = -\kappa \mathbf{t} + \tau \mathbf{b} ; \quad \mathbf{b}_s = -\tau \mathbf{n}, \quad (1)$$

where the subscript  $s$  stands for derivative with respect to  $s$ . In addition, the curvature of the curve is  $\kappa = |\mathbf{t}_s|$ , and its torsion  $\tau = [\mathbf{t} \cdot (\mathbf{t}_s \times \mathbf{t}_{ss})]/\kappa^2$  which is a measure of the nonplanarity of the curve. Further, Eqs. (1) can be combined to give  $\boldsymbol{\sigma}_s = \boldsymbol{\omega}_D \times \boldsymbol{\sigma}$ , where  $\boldsymbol{\sigma}$  stands for  $\mathbf{t}, \mathbf{n}$  or  $\mathbf{b}$ , and  $\boldsymbol{\omega}_D = \tau \mathbf{t} + \kappa \mathbf{b}$  is called the Darboux vector. Thus the Frenet frame made up of the orthogonal unit triad  $[\mathbf{t}, \mathbf{n}, \mathbf{b}]$  *rotates* with an angular velocity  $\boldsymbol{\omega}_D$ , as one moves along the curve parametrized by  $s$ .

Using the definitions given below Eq. (1), we find the curvature  $\kappa$  and the torsion  $\tau$  for the helix to be  $\kappa = k_0 = \alpha^2 R_0$  and  $\tau = \tau_0 = \alpha^2 P_0/2\pi$ . These yield  $k_0/\tau_0 = 2\pi R_0/P_0$ , and

$$\alpha = \sqrt{(k_0^2 + \tau_0^2)}. \quad (2)$$

Hence, for a helix the curvature and torsion are constants determined by its radius and its pitch.

It is convenient to write all the relevant quantities for the helix in terms of  $k_0$  and  $\tau_0$  using the above relationships. Thus the parametric equation for the helix becomes

$$\mathbf{R}(s) = (1/\alpha^2)[k_0 \cos \alpha s, k_0 \sin \alpha s, \tau_0 \alpha s]. \quad (3)$$

From Eq. (3) we find

$$\mathbf{t}(s) = d\mathbf{R}(s)/ds = [-k_0 \sin \alpha s, k_0 \cos \alpha s, \tau_0]/\alpha. \quad (4)$$

Using Eq. (4) in Eqs. (1) with  $k = k_0$  and  $\tau = \tau_0$ , we find the normal vector  $\mathbf{n}$  and the binormal vector  $\mathbf{b}$  for the helix to be

$$\mathbf{n}(s) = \mathbf{t}_s/|\mathbf{t}_s| = [-\cos \alpha s, -\sin \alpha s, 0] \quad ; \quad \mathbf{b}(s) = [\tau_0 \sin \alpha s, -\tau_0 \cos \alpha s, k_0]/\alpha, \quad (5)$$

where  $\alpha$  is defined in Eq. (2). The length of a helix with integer  $q$  turns of  $2\pi$  is given by

$$L(q) = 2\pi q / \sqrt{(k_0^2 + \tau_0^2)}, \quad (6)$$

where  $q = 1, 2, 3, \dots$

The surfaces of the *normal and binormal helical ribbons* are constructed, respectively, using the following position vectors  $\mathbf{X}^{(n)}(s, \xi)$  and  $\mathbf{X}^{(b)}(s, \xi)$  parametrized by  $s$  and  $\xi$ :

$$\mathbf{X}^{(n)}(s, \xi) = \mathbf{R}(s) - \xi \mathbf{n}(s) \quad (7)$$

and

$$\mathbf{X}^{(b)}(s, \xi) = \mathbf{R}(s) + \xi \mathbf{b}(s). \quad (8)$$

In the above,  $\mathbf{R}(s)$  is the central helix on the ribbon, given in Eq. (3). The vectors  $\mathbf{n}$  and  $\mathbf{b}$  for this helix were found in Eq. (5). The arc length  $s = [0, L]$  ( $L$  =length of the helix) and  $\xi$  is the parameter along the width of the ribbon (which is in the local normal and binormal direction, respectively, for the two types of ribbon), with  $\xi = [-d, d]$ . Here  $2d$  is the width of the ribbon.

### 3 Geometric parameters for normal and binormal helical ribbons

As is well known [13], the geometry of a 2D surface created by a position vector  $\mathbf{X}(s, \xi)$  depends on two quadratic differential forms. The First fundamental form denoted by I is just the local metric on the surface given by  $I = (d\mathbf{X})^2 = E ds^2 + 2F ds d\xi + G d\xi^2$ , where

$$E = \mathbf{X}_s \cdot \mathbf{X}_s ; \quad F = \mathbf{X}_s \cdot \mathbf{X}_\xi ; \quad G = \mathbf{X}_\xi \cdot \mathbf{X}_\xi. \quad (9)$$

The unit normal  $\mathbf{N}(s, \xi)$  at every point  $(s, \xi)$  on a surface  $\mathbf{X}(s, \xi)$  is defined as

$$\mathbf{N}(s, \xi) = \frac{(\mathbf{X}_s \times \mathbf{X}_\xi)}{|\mathbf{X}_s \times \mathbf{X}_\xi|} = \frac{(\mathbf{X}_s \times \mathbf{X}_\xi)}{\sqrt{EG - F^2}}. \quad (10)$$

The second fundamental form denoted by II encodes how the 2D surface is embedded in the ambient 3D space. It is a measure of how the normal vector to the surface  $\mathbf{N}$  varies as one moves on the surface. It is given by  $II = -d\mathbf{X} \cdot d\mathbf{N} = e ds^2 + 2f ds d\xi + g d\xi^2$ , where

$$e = -\mathbf{X}_s \cdot \mathbf{N}_s = \mathbf{X}_{ss} \cdot \mathbf{N} ; \quad f = -\mathbf{X}_s \cdot \mathbf{N}_\xi = -\mathbf{X}_\xi \cdot \mathbf{N}_s ; \quad g = -\mathbf{X}_\xi \cdot \mathbf{N}_\xi. \quad (11)$$

Gaussian curvature  $K$  and mean curvature  $M$  of the surface are given in terms of  $E, F, G, e, f, g$  as [13]

$$K = (eg - f^2)/(EG - F^2); \quad M = (gE - 2fF + eG)/2(EG - F^2). \quad (12)$$

Next, we use all the above expressions to obtain the various geometrical parameters for the normal and binormal helical ribbons given in Eqs. (7) and (8). We use the superscripts  $(n)$  and  $(b)$  to denote quantities pertaining to a *normal* and a *binormal* helical ribbon, respectively.

Differentiating Eqs. (7) and (8) with respect to  $s$  and  $\xi$  respectively, and using the Frenet-Serret equations (1) for the helix (with  $\kappa = \kappa_0$  and  $\tau = \tau_0$ ), we get

$$\mathbf{X}_s^{(n)} = (1 + k_0\xi)\mathbf{t} - \xi\tau_0\mathbf{b}; \quad \mathbf{X}_\xi^{(n)} = -\mathbf{n}; \quad \mathbf{X}_s^{(b)} = \mathbf{t} - \xi\tau_0\mathbf{n}; \quad \mathbf{X}_\xi^{(b)} = \mathbf{b}. \quad (13)$$

Using the above in Eq. (9), we obtain

$$E^{(n)}(\xi) = [(1 + k_0\xi)^2 + \tau_0^2\xi^2] = [1 + 2k_0\xi + (k_0^2 + \tau_0^2)\xi^2]; \quad F^{(n)} = 0; \quad G^{(n)} = 1 \quad (14)$$

and

$$E^{(b)}(\xi) = 1 + \tau_0^2\xi^2; \quad F^{(b)} = 0; \quad G^{(b)} = 1. \quad (15)$$

Hence the metrics for the normal and binormal helical ribbons are given by  $[d\mathbf{X}^{(n)}]^2 = E^{(n)}(\xi)ds^2 + d\xi^2$  and  $[d\mathbf{X}^{(b)}]^2 = E^{(b)}(\xi)ds^2 + d\xi^2$ , respectively.

On using Eq. (13) in Eq. (10), we find the surface normals of the normal and binormal helical ribbons to be

$$\mathbf{N}^{(n)} = [-(1 + k_0\xi)\mathbf{b} - \xi\tau_0\mathbf{t}] / \sqrt{E^{(n)}(\xi)}; \quad \mathbf{N}^{(b)} = [-\mathbf{n} - \xi\tau_0\mathbf{t}] / \sqrt{E^{(b)}(\xi)}. \quad (16)$$

A short calculation yields

$$\mathbf{N}_s^{(n)} = \tau_0\mathbf{n} / \sqrt{E^{(n)}(\xi)}; \quad \mathbf{N}_\xi^{(n)} = [\tau_0^2\xi\mathbf{b} - \tau_0(1 + k_0\xi)\mathbf{t}] / (E^{(n)})^{3/2}; \quad \mathbf{N}_s^{(b)} = [k_0\mathbf{t} - \tau_0\mathbf{b} - \xi\tau_0k_0\mathbf{n}] / \sqrt{E^{(b)}(\xi)}, \quad (17)$$

while  $\mathbf{N}_\xi^{(b)}$  is found to be a vector with components only along  $\mathbf{t}$  and  $\mathbf{n}$ . Next, using Eqs. (13) and (17) in Eq. (11) we obtain

$$e^{(n)} = 0; \quad f^{(n)} = \tau_0 / \sqrt{E^{(n)}}; \quad g^{(n)} = 0 \quad (18)$$

and

$$e^{(b)} = -k_0 \sqrt{E^{(b)}(\xi)}; \quad f^{(b)} = \tau_0 / \sqrt{E^{(b)}(\xi)} \quad ; \quad g^{(b)} = 0. \quad (19)$$

By substituting Eqs. (14) and (18) for the normal ribbon, and Eqs. (15) and (19) for the binormal ribbon respectively in Eq.(12), we obtain the respective expressions for the Gaussian curvature  $K$  and the mean curvature  $M$ . Using them, the quantity  $(M^2 - K)$  is found. We get

$$K^{(n)} = -\tau_0^2 / [E^{(n)}(\xi)]^2; \quad M^{(n)} = 0; \quad [M^{(n)}]^2 - K^{(n)} = \frac{\tau_0^2}{[E^{(n)}(\xi)]^2} \quad (20)$$

for the normal helical ribbon, and

$$K^{(b)} = -\tau_0^2 / [E^{(b)}(\xi)]^2; \quad M^{(b)} = -k_0 / 2 \sqrt{E^{(b)}(\xi)}; \quad [M^{(b)}]^2 - K^{(b)} = \frac{k_0^2}{4E^{(b)}(\xi)} + \frac{\tau_0^2}{(E^{(b)}(\xi))^2} \quad (21)$$

for the binormal helical ribbon.

Since the mean curvature  $M^{(n)}$  vanishes for the normal helical ribbon, it represents a minimal surface. The quantity  $(M^2 - K)$  will play an important role in the study of quantum particle transport on both the helical ribbons.

## 4 Quantum particle transport on normal and binormal helical ribbons

### 4.1 Schrödinger equation for a particle on a general curved 2D surface

In a seminal paper, da Costa [12] has presented a consistent formulation for studying the quantum mechanics of a particle constrained to move on a two dimensional curved surface  $\mathbf{X}(s, \xi)$  embedded in a three dimensional space. A lengthy and detailed analysis yields the following time-independent Schrödinger equation for the surface wave function  $\chi(s, \xi)$ , valid for *all surfaces* with orthogonal curvilinear coordinates, i.e.,  $F = \mathbf{X}_s \cdot \mathbf{X}_\xi = 0$  in the surface metric:

$$-\frac{\hbar^2}{2m} \frac{1}{h_1 h_2} \left[ \frac{\partial}{\partial s} \frac{h_2}{h_1} \frac{\partial \chi}{\partial s} + \frac{\partial}{\partial \xi} \frac{h_1}{h_2} \frac{\partial \chi}{\partial \xi} \right] - \frac{\hbar^2}{2m} [M^2 - K] \chi = \mathcal{E} \chi, \quad (22)$$

where  $h_1, h_2$  are the Lamé coefficients. Here  $M$  and  $K$  are the mean curvature and Gaussian curvature for the surface.



## 4.2 Schrödinger equation on the surface of helical ribbons

As seen from the last entry in Eqs. (20) and (21) respectively, the quantity  $(M^2 - K)$  appearing in Eq. (22) is expressed in terms of the respective surface metric parameters  $E(\xi)$ , for *both* normal and binormal ribbons. In the case of these helical ribbons, it is therefore convenient to express the Lamé coefficients  $h_1$  and  $h_2$  appearing in Eq. (22) in terms of  $E(\xi)$ . As shown in Eqs. (14) and (15),  $F = 0$  and  $G = 1$  for both ribbons. Thus the surface metric is given by  $(d\mathbf{X})^2 = h_1^2 ds^2 + h_2^2 d\xi^2 = E(\xi) ds^2 + d\xi^2$ , yielding  $h_1 = \sqrt{E(\xi)}$  and  $h_2 = 1$  for both ribbons. Using these in Eq. (22), we obtain

$$-\frac{\hbar^2}{2m} \frac{1}{\sqrt{E}} \left[ \frac{\partial}{\partial s} \frac{1}{\sqrt{E}} \frac{\partial \chi}{\partial s} + \frac{\partial}{\partial \xi} \sqrt{E} \frac{\partial \chi}{\partial \xi} \right] - \frac{\hbar^2}{2m} [M^2 - K] \chi = \mathcal{E} \chi. \quad (23)$$

Note that the Schrödinger equation given in Eq. (23) is valid for *both* normal and binormal ribbons. Therefore, we will proceed to analyze this equation in terms of  $E(\xi)$  using this general form valid for both ribbons. In the final results we will substitute the corresponding expressions for  $E(\xi)$  and  $(M^2 - K)$  for the normal ribbon from Eqs. (14) and (20), and for the binormal ribbon from Eqs. (15) and (21).

Since the curved surface area element of the ribbon concerned is  $da = h_1 ds d\xi = \sqrt{E(\xi)} ds d\xi$ , a normalized wave function  $\Phi(s, \xi)$  should satisfy

$$\chi(s, \xi) = \frac{\Phi(s, \xi)}{\sqrt{h_1}} = \frac{\Phi(s, \xi)}{[E(\xi)]^{1/4}}, \quad (24)$$

so that  $\int \int |\Phi|^2 ds d\xi = 1$ . Substituting Eq. (24) into Eq. (23), a lengthy but straightforward calculation yields

$$-\frac{\hbar^2}{2m} \frac{1}{E(\xi)} \frac{\partial^2 \Phi}{\partial s^2} - \frac{\hbar^2}{2m} \frac{\partial^2 \Phi}{\partial \xi^2} + V_{eff}(\xi) \Phi = \mathcal{E} \Phi, \quad (25)$$

where  $V_{eff}(\xi)$  is given by

$$V_{eff}(\xi) = -\frac{\hbar^2}{2m} \left[ \frac{3(E_\xi)^2}{16E^2(\xi)} - \frac{E_{\xi\xi}}{4E(\xi)} + (M^2 - K) \right]. \quad (26)$$

Here  $E_\xi$  and  $E_{\xi\xi}$  represent the first and second derivatives of  $E$  with respect to  $\xi$ , respectively. After multiplying both sides of Eq. (25) by  $E(\xi)$ , we look for a separable solution of the form

$$\Phi(s, \xi) = u(s)w(\xi). \quad (27)$$

Dividing the resulting equation by  $u(s)w(\xi)$ , we get a separable form for the Schrödinger equation, which enables us to write

$$-\frac{\hbar^2}{2m} \frac{\partial^2 u}{\partial s^2} = \mathcal{E}_0 u(s). \quad (28)$$

Substituting Eq. (28) in the separable form we obtained, multiplying the resulting equation by  $w(\xi)/E(\xi)$  and rearranging the terms leads to the following Schrödinger equation for the wave function  $w(\xi)$

$$-\frac{\hbar^2}{2m} \frac{\partial^2 w(\xi)}{\partial \xi^2} + \left[ V_{eff}(\xi) + \frac{\mathcal{E}_0}{E(\xi)} \right] w(\xi) = \mathcal{E} w(\xi). \quad (29)$$

Thus in the above Schrödinger equation, the effective potential is given by

$$U_{eff}(\xi, \mathcal{E}_0) = \left[ V_{eff}(\xi) + \frac{\mathcal{E}_0}{E(\xi)} \right], \quad (30)$$

where  $V_{eff}(\xi)$  is given in Eq. (26).

### 4.3 Effective quantum geometric potential: Helical ribbon of finite Length

The effective potential given by Eq. (30) depends upon the quantity  $\mathcal{E}_0$  which is to be found by solving Eq. (28) for appropriate boundary conditions [23] on the wave function  $u(s)$ . As should be clear, for a particle confined to a helical ribbon of length  $L$ , the wave function  $u(s)$  must vanish at the two ends of the ribbon, giving the boundary condition  $u(0) = u(L) = 0$ . For the solution  $u(s) = u_0 \sin ks$ , this condition yields

$$k = k_n = n\pi/L, \quad (31)$$

where  $n = 1, 2, 3, \dots$ . Hence only *nonzero* quantized values of  $k$  are allowed for both types of helical ribbons, implying the existence of *only moving particles*.

A helical ribbon with length  $L$  which is composed of integer  $q$  complete  $2\pi$  turns of the helix presents an interesting special case. Here,  $L = L(q) = 2\pi q / \sqrt{(k_0^2 + \tau_0^2)}$  (see Eq. (6)) so that Eq. (31) becomes

$$k = k_{n,q} = n\pi/L(q) = (n/2q) \sqrt{(k_0^2 + \tau_0^2)}, \quad (32)$$

where  $n = 1, 2, 3, \dots$  and  $q = 1, 2, 3, \dots$ . For this case, the quantized value of  $k$  depends on two nonzero integers  $n$  and  $q$ , leading to a rich behavior. We will therefore focus on the effective quantum geometric potential for such ribbons.

Thus Eq. (28) yields  $\mathcal{E}_0 = \frac{\hbar^2 k^2}{2m} = \frac{\hbar^2 k_{n,q}^2}{2m}$ . Substituting for  $\mathcal{E}_0$  in Eq. (29), the Schrödinger equation for  $w(\xi)$  becomes

$$-\frac{\hbar^2}{2m} \frac{\partial^2 w(\xi)}{\partial \xi^2} + U_{eff}(\xi, k_{n,q}) w(\xi) = \mathcal{E} w(\xi), \quad (33)$$

where the effective potential  $U_{eff}(\xi, k_{n,q})$  is given by

$$U_{eff}(\xi, k_{n,q}) = -\frac{\hbar^2}{2m} \left[ \frac{3(E_\xi)^2}{16E^2(\xi)} - \frac{E_{\xi\xi}}{4E(\xi)} + (M^2 - K) - \frac{k_{n,q}^2}{E(\xi)} \right]. \quad (34)$$

The effective potential given in (34) is seen to be purely quantum mechanical in origin [24, 25] since it is proportional to  $\hbar^2$ . In addition, it is also dependent on the *surface geometric parameters*  $E$  and  $(M^2 - K)$  for the respective ribbons. Hence  $U_{eff}(\xi, k_{n,q})$  is called the *effective quantum geometric potential*.

As mentioned below Eq. (23), the Schrödinger equation, Eq. (33), is valid for *both* the normal and binormal ribbons. To obtain their respective effective potentials, the corresponding expressions for the geometric parameters for the normal and binormal ribbons should be substituted on the right hand side of  $U_{eff}(\xi, k_{n,q})$  given in (34).

For the normal and binormal ribbons, from Eqs. (14) and (15) we have

$$E^{(n)}(\xi) = [(1 + k_0\xi)^2 + \tau_0^2\xi^2] = [1 + 2k_0\xi + (k_0^2 + \tau_0^2)\xi^2] ; \quad E_\xi^{(n)} = 2[k_0 + (k_0^2 + \tau_0^2)\xi] ; \quad E_{\xi\xi}^{(n)} = 2(k_0^2 + \tau_0^2) \quad (35)$$

and

$$E^{(b)}(\xi) = (1 + \tau_0^2\xi^2) ; \quad E_\xi^{(b)} = 2\tau_0^2\xi ; \quad E_{\xi\xi}^{(b)} = 2\tau_0^2. \quad (36)$$

In Eq. (34), substituting the expressions for  $(M^2 - K)$  given in the last entry of Eq. (20) [resp. Eq. (21)] with Eq. (35) [resp. Eq. (36)] for the normal [resp. binormal] helical ribbon, a very lengthy calculation yields an effective quantum geometric potential which is given by the following *same functional of*  $E(\xi)$  for both the normal and binormal helical ribbons.

$$U_{eff}(\xi, k_{n,q}) = -\frac{\hbar^2}{8m} \left[ \frac{[(k_0^2 + \tau_0^2) - 4k_{n,q}^2]}{E(\xi)} + \frac{\tau_0^2}{[E(\xi)]^2} \right], \quad (37)$$

where  $k_{n,q}$  is defined in Eq. (32).

An inspection of our detailed calculations shows that this similarity in the functional form for *both* ribbons arises from the intricate interplay between contributions to the quantum potential arising from

the (intrinsic) surface metric part  $E$ , and the (extrinsic) part  $[(M^2 - K)]$  [see Eqs. (20) and (21)] in the expression for the effective potential given in Eq. (34).

Summarizing, to find the effective quantum geometric potentials for the normal and binormal helical ribbons, we only need to substitute in Eq. (37), the respective expressions for  $E(\xi)$  for these ribbons which are given in the first entries in Eqs. (35) and (36). We note that  $E^{(n)}(\xi)$  and  $E^{(b)}(\xi)$  are positive for all  $\xi$ . As is clear from Eq. (33), localized states are supported when the effective potential  $U_{eff}(\xi, k_{n,q})$  given in Eq. (37) takes on *negative* values for all  $\xi$ . Additionally, Eq. (32) shows that  $k_{n,q}$  is always nonzero. This leads to the following *geometric condition* on  $k_{n,q}$  for the existence of localized states:

$$0 < k_{n,q}^2 \leq \frac{(k_0^2 + \tau_0^2)}{4}. \quad (38)$$

We find it convenient to write Eq. (37) in the form

$$U_{eff}(\xi, \beta_{n,q}) = -\frac{\hbar^2}{2m} \left[ \frac{\beta_{n,q}(k_0^2 + \tau_0^2)}{E(\xi)} + \frac{\tau_0^2}{4E^2(\xi)} \right], \quad (39)$$

where the parameter  $\beta_{n,q}$  is defined as

$$\beta_{n,q} = \frac{1}{4} - \frac{k_{n,q}^2}{(k_0^2 + \tau_0^2)}. \quad (40)$$

Thus the condition for localized states given in Eq. (38) becomes  $0 \leq \beta_{n,q} < \frac{1}{4}$ .

Substituting Eq. (32) in Eq. (40) yields

$$\beta_{n,q} = \frac{1}{4} \left( 1 - \frac{n^2}{q^2} \right). \quad (41)$$

Using Eq. (41), the quantum effective geometric potential given in Eq. (39) becomes

$$U_{eff}(\xi, n, q) = -\frac{\hbar^2}{8m} \left[ \frac{(k_0^2 + \tau_0^2) \left( 1 - \frac{n^2}{q^2} \right)}{E(\xi)} + \frac{\tau_0^2}{E^2(\xi)} \right], \quad (42)$$

where  $n = 1, 2, 3, \dots, q$  and  $q = 1, 2, 3, \dots$ . Hence the condition for *localized states* becomes

$$1 \leq n^2 \leq q^2. \quad (43)$$

This gives the intriguing result that the particle momentum quantum number for localized states is restricted by the integer  $q$ .

We note that since the metric for the normal ribbon  $E^{(n)}(\xi)$  is greater than the metric for the binormal ribbon  $E^{(b)}(\xi)$ , Eq. (42) shows that these states satisfy

$$U_{eff}^{(n)}(\xi, n, q) < U_{eff}^{(b)}(\xi, n, q). \quad (44)$$

#### 4.4 Analysis of the effective quantum geometric potential

We now analyze the expression for the effective quantum geometric potential  $U_{eff}(\xi, \beta_{n,q})$  given in Eq. (39). It is convenient to use the notation  $\beta$  for  $\beta_{n,q}$  in the following analysis. We define

$$C_0 = 4\beta(k_0^2 + \tau_0^2). \quad (45)$$

We are mainly concerned with *localized states* in this paper. For these states,  $C_0 \geq 0$ , as seen from Eq. (41). Next, (setting the constant  $\hbar^2/2m = 1$  for convenience) we write the potential in Eq. (39) as  $U_{eff}(\xi) = -\frac{1}{4E^2(\xi)}[C_0E(\xi) + \tau_0^2]$ . This yields

$$\frac{dU_{eff}}{d\xi} = \frac{1}{4E^3(\xi)}E_\xi [C_0E(\xi) + 2\tau_0^2], \quad (46)$$

where  $E_\xi = dE/d\xi$ . Hence the extrema of  $U_{eff}(\xi, k)$  are given by either (a)  $E_\xi = 0$  or (b)  $[C_0E(\xi) + 2\tau_0^2] = 0$ . Since  $E(\xi)$  is a quadratic function of  $\xi$  for both ribbons, Case (a) leads to one extremum and Case (b) to two extrema. However, for localized states, we must have  $C_0 \geq 0$  as mentioned above. Further,  $E(\xi)$  is positive definite for both ribbons. Hence the extremum condition for Case (b) cannot be satisfied for localized states.

Now, Case (a) corresponds to  $E_\xi = 0$ . On using Eqs. (35) and (36), we find that the single extremum for the normal and binormal helical ribbon appears, respectively, at

$$\xi^{(n)} = \xi_0^{(n)} = -\frac{k_0}{(k_0^2 + \tau_0^2)} \quad ; \quad \xi^{(b)} = \xi_0^{(b)} = 0. \quad (47)$$

Next, we calculate

$$\frac{d^2U_{eff}}{d\xi^2} = \frac{1}{4E^6(\xi)} \left[ E^3(\xi)[C_0E(\xi) + 2\tau_0^2]E_{\xi\xi} - 2E^2[C_0E(\xi) + 3\tau_0^2]E_\xi^2 \right]. \quad (48)$$

On setting  $E_\xi = 0$  in Eq. (48), we find that  $\frac{d^2U_{eff}}{d\xi^2} > 0$ , since  $C_0 \geq 0$  for localized states. Hence the extremum given in Eq. (47) is a *minimum* for both ribbons.

Although Case (b) is not relevant for the localized states we are concerned with, for completeness we also discuss this case. Here, the extremum condition is  $[C_0 E(\xi) + 2\tau_0^2] = 0$ , whose two roots correspond to two extrema. Let us denote them by  $\xi_{\pm}$ . Now, substituting this condition in Eq. (48), we find that at  $\xi = \xi_{\pm}$ ,  $\frac{d^2 U_{eff}}{d\xi^2} = -[2E^2(\xi)\tau_0^2 E_{\xi}^2] < 0$ , showing that these two extrema will always be *maxima*. Our further analysis shows that two well-separated, shallow positive maxima of equal height appear at  $\xi_+$  and  $\xi_-$  for  $\beta > 0$ , which *approach each other*, increasing in height with increasing  $n$  to merge into a single positive maximum.

The above analytical results agree with Figs. 1 and 2, where we have plotted the quantum effective potential  $U_{eff}(\xi, \beta_{n,q})$  given in Eq. (39), as a function of  $\xi$ , for the normal and binormal ribbon, respectively. In Figs. 3 and 4, we depict the normal and binormal helical ribbons, respectively. We find that the particle localizes near the inner edge for the normal helical ribbon, and on the central helix for the binormal helical ribbon, in agreement with Figs. 1 and 2.

## 5 Quantum analog of the Coriolis effect in a helical nanoribbon

As analytically shown in Sec. (4.4) and illustrated in Figs. 1 and 2, a single minimum of the effective quantum geometric potential occurs at  $\xi = \xi_{min}^{(n)} = -\frac{k_0}{(k_0^2 + \tau_0^2)}$  for the normal helical ribbon, and at  $\xi = \xi_{min}^{(b)} = 0$ , for the binormal helical ribbon. Further, it was shown in In Sec. (4.3) that for a quantum particle confined to a helical ribbon of any finite length, the wave vector  $k$  takes on quantized *nonzero* values. Thus we have only a moving particle on such a ribbon.

Such a localization of a moving particle on a helical curve at a specific width  $\xi = \xi_{min}$  for each helical ribbon suggests the presence of a pseudo-force acting on the particle (with wave function  $u(s)$  satisfying Eq. (28)) moving along the tangent vector  $\mathbf{X}_s(s, \xi)$  to the  $s$ -curve on the surface of the ribbon, which deflects the particle transversely along the width  $\xi$  of the ribbon concerned. (Transverse, because  $\mathbf{X}_s \cdot \mathbf{X}_{\xi} = 0$  for both types of helical ribbons.)

This force is highly reminiscent of the fictitious Coriolis force  $\mathbf{F}_{cor}$  on a classical particle moving with velocity  $\mathbf{v}$  in a non-inertial frame rotating with an angular velocity  $\mathbf{\Omega}$  with respect to an inertial frame,

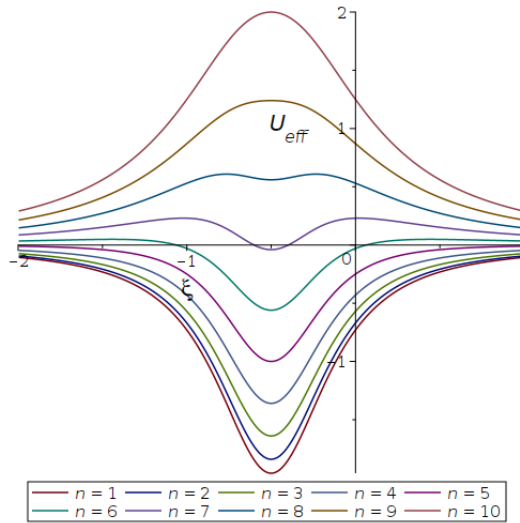


Figure 1: Plots for the effective quantum geometric potential  $U_{eff}(\xi, \beta_{n,q})$  for the normal helical ribbon given in Eq. (39) [setting  $\hbar^2/2m = 1$ ] as a function of  $\xi$ , with  $E(\xi) = E^{(n)}(\xi)$  given in Eq. (14).  $\beta_{n,q} = \frac{1}{4}(1 - \frac{n^2}{q^2})$ . We choose  $k_0 = \tau_0 = 1$  and  $q = 5$ . Plots from bottom to top correspond to moving particles with quantum numbers  $n = 1, 2, \dots, 10$ . For  $n \leq 5$ , the moving particle localizes at the minimum given by  $\xi_{min} = -k_0/(k_0^2 + \tau_0^2) = -0.5$ . For  $n > 5$ , two maxima start to appear on either side of the minimum, and approach each other as  $n$  increases further to become a single maximum, as shown analytically in Sec. (4.4).

which transversely deflects the particle. For a particle with mass  $m$ , it is given by [20]

$$\mathbf{F}_{cor} = -2m \mathbf{\Omega} \times \mathbf{v}. \quad (49)$$

In what follows, we investigate whether the quantum particle localization at specific widths for each ribbon, which is essentially caused by the quantum geometric potential  $U_{eff}(\xi, \beta)$  given in Eq. (39) can be cast in the form given in Eq. (49), so that this phenomenon can be regarded as a quantum analog of the (classical) Coriolis effect [21].

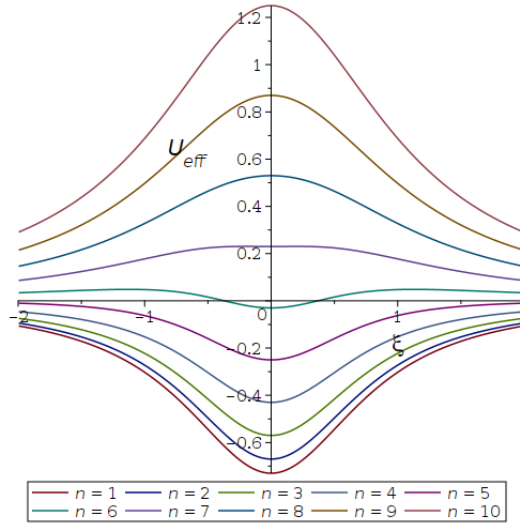


Figure 2: Plots for the effective quantum geometric potential  $U_{eff}(\xi, \beta_{n,q})$  for the binormal helical ribbon given in Eq. (39) [setting  $\hbar^2/2m = 1$ ] as a function of  $\xi$ , with  $E(\xi) = E^{(b)}(\xi)$  given in Eq. (15).  $\beta_{n,q} = \frac{1}{4}(1 - \frac{n^2}{q^2})$ . We choose  $k_0 = \tau_0 = 1$  and  $q = 5$ . Plots from bottom to top correspond to moving particles with quantum numbers  $n = 1, 2, \dots, 10$ . For  $n \leq 5$ , the moving particle localizes at the minimum given by  $\xi_{min} = 0$ . For  $n > 5$ , two maxima start to appear on either side of the minimum, and approach each other as  $n$  increases further, to become a single maximum, as shown analytically in Sec. (4.4).

### 5.1 General methodology applicable to both types of ribbons

Our aim is to show that an equation analogous to Eq. (49) can be written down for a quantum particle moving on a helical ribbon. We accomplish this by identifying the quantum analog of each of the terms appearing in that equation.

We have seen that a helical ribbon of any finite length supports *only* moving quantum particles. We find the quantum analog of  $m\mathbf{v}$  on a helical ribbon appearing on the RHS of Eq. (49) as follows.

Let  $\mathbf{X}$  denote the surface of a helical ribbon. (See Eqs. (7) and (8).) Let the quantum particle satisfying Eq. (28) move along the helical  $s$ -curve at a given point  $\xi$  lying on the width of the ribbon, with velocity  $\mathbf{v}$ . As should be clear,

$$\mathbf{v} = v \frac{\mathbf{X}_s}{|\mathbf{X}_s|} = v \hat{\mathbf{T}}(s, \xi), \quad (50)$$



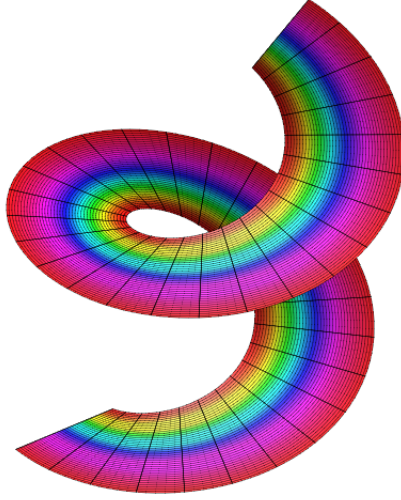


Figure 3: Normal helical ribbon. Width parameter  $\xi$  for the ribbon is in the range  $-0.5 < \xi < 0.33$ . The coloring of the surface corresponds to the magnitude of the effective geometric potential (see Fig. 1) for a quantum particle with  $n = 1$ . Only one turn of the ribbon is displayed. Particle localization, which corresponds to the minimum of the potential, is near the inner edge of the ribbon as highlighted in red. This is in agreement with Fig. 1.

where

$$\hat{\mathbf{T}}(s, \xi) = \frac{\mathbf{X}_s}{|\mathbf{X}_s|} \quad (51)$$

is the unit tangent vector along the  $s$ -curve at a specific width coordinate  $\xi$ .

Using the well known de Broglie relation  $mv = \hbar k$ , we obtain the *quantum analog* of  $m\mathbf{v}$  appearing on the RHS of Eq. (49) as

$$m\mathbf{v} = \hbar k \hat{\mathbf{T}}(s, \xi). \quad (52)$$

Since we are only concerned with *localized states* for the wave function, we are justified in invoking the Ehrenfest theorem [22] to write the *quantum analog* of the force deflecting the quantum particle transversely

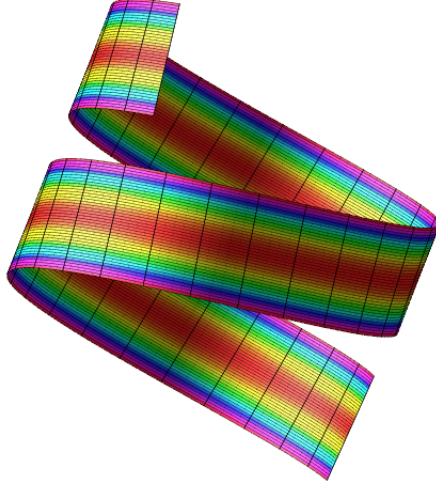


Figure 4: Binormal helical ribbon. Width parameter  $\xi$  for the ribbon is in the range  $-0.33 < \xi < 0.33$ . The coloring of the surface corresponds to the magnitude of the effective geometric potential (see Fig. 2 ) for a quantum particle with  $n = 1$ . Only one turn of the ribbon is displayed. Particle localization, which corresponds to the minimum of the potential, is on the central helix of the ribbon as highlighted in red. This is in agreement with Fig. 2.

on a helical ribbon as the negative gradient of the corresponding potential function. Thus we obtain

$$\mathbf{F}_Q = -[dU_{eff}(\xi, \beta)/d\xi] \hat{\xi}, \quad (53)$$

where the effective quantum geometric potential  $U_{eff}(\xi, \beta)$  is given in Eq. (39). In Eq. (53), we have also used the fact that the direction of the force that pushes the particle along the width of the ribbon is just the ‘unit width vector’  $\hat{\xi} = \xi/|\xi|$  in the  $\xi$  direction. From the definition of the two ribbons given in Eqs. (7) and (8), we see that  $\xi$  is along  $\mathbf{n}$  and  $\mathbf{b}$  respectively, for the normal and binormal ribbons.

From Eq. (46), we write the following general expression for  $[dU_{eff}(\xi, \beta)/d\xi]$  appearing in Eq. (53) as

$$-[dU_{eff}(\xi, \beta)/d\xi] = -[\hbar^2/2m]G(\xi, \beta)(dE/d\xi), \quad (54)$$

where  $G(\xi, \beta)$  is given by

$$G(\xi, \beta) = [C_0 E(\xi) + 2\tau_0^2]/4E^3(\xi) = [4\beta(k_0^2 + \tau_0^2) E(\xi) + 2\tau_0^2]/4E^3(\xi). \quad (55)$$

In the above, we have substituted for  $C_0$  from Eq. (45). From Eq. (40), we have  $\beta = \frac{1}{4} - \frac{k^2}{(k_0^2 + \tau_0^2)}$ , on suppressing the quantum indices  $n$  and  $q$  on  $\beta$  and  $k$  for convenience. Substituting for  $\beta$  we get

$$G(\xi, \beta) = G(k, \xi) = \left[ (k_0^2 + \tau_0^2) \left( 1 - \frac{4k^2}{(k_0^2 + \tau_0^2)} \right) E(\xi) + 2\tau_0^2 \right] / 4E^3(\xi). \quad (56)$$

In Eq. (54), we have re-introduced the factor  $[\hbar^2/2m]$  which had earlier been set to unity in the potential in Sec. (4.4) for calculational convenience. As is clear, Eq. (54) is valid for both ribbons, with the appropriate expressions for  $E(\xi)$  substituted for the respective ribbons.

Substituting Eq. (54) in Eq. (53) we obtain the quantum analog of the force that is pushing the particle in the transverse direction to be

$$\mathbf{F}_Q = -[\hbar^2/2m]G(k, \xi)(dE/d\xi) \hat{\xi} \quad (57)$$

where  $G(k, \xi)$  is given in Eq. (56).

In order to interpret Eq. (57) as a quantum analog of the Coriolis force, we should be able to write it in the form of Eq. (49) and find the quantum analog of the angular velocity  $\boldsymbol{\Omega}$ . To this end, we first substitute the quantum analog of  $m\mathbf{v}$  given in Eq. (52), along with the quantum analog  $\mathbf{F}_Q$  given in Eq. (57) into Eq. (49). We then proceed to identify the *quantum analog* of the angular velocity denoted by  $\boldsymbol{\Omega}_Q$  in such a way that it satisfies

$$\mathbf{F}_Q = -[\hbar^2/2m]G(k, \xi)(dE/d\xi) \hat{\xi} = \boldsymbol{\Omega}_Q \times -2\hbar k \hat{\mathbf{T}}(s, \xi). \quad (58)$$

This yields

$$[\hbar/(4mk)]G(k, \xi)(dE/d\xi) \hat{\xi} = \boldsymbol{\Omega}_Q \times \hat{\mathbf{T}}(s, \xi) \quad (59)$$

where  $G(k, \xi)$  is given in Eq. (56). In the above, the quantities  $\hat{\mathbf{T}}(s, \xi)$ ,  $G(k, \xi)$ ,  $E(\xi)$  and  $\hat{\xi}$  are ribbon-dependent, and will be explicitly computed for the normal and binormal helical ribbons. Using them in Eq. (59), enables us to identify the *quantum analogs* ( $\boldsymbol{\Omega}_Q$ ) of the respective angular velocities of the rotating (non-inertial) Coriolis frames for the two types of ribbons, as we show below.

## 5.2 Angular velocities of rotating frames for normal and binormal helical ribbons

We will use the superscripts  $(n)$  and  $(b)$  to denote quantities pertaining to the normal and binormal helical ribbons respectively.

**Normal helical ribbon:** From the general expression for  $\hat{\mathbf{T}}(s, \xi)$  given in (51), a short calculation using the definition Eq. (7), along with the Frenet-Serret equations, Eq. (1), for the helix yields

$$\hat{\mathbf{T}}^{(n)}(s, \xi) = \frac{\mathbf{X}_s^{(n)}}{|\mathbf{X}_s^{(n)}|} = [(1 + k_0\xi)\mathbf{t} - \tau_0\xi\mathbf{b}]/E^{(n)}(\xi). \quad (60)$$

Since  $\hat{\boldsymbol{\xi}} = \mathbf{n}$  for the normal ribbon, the LHS of Eq. (59) is a vector along  $\mathbf{n}$ . The vector  $\hat{\mathbf{T}}^{(n)}(s, \xi)$  appearing on its RHS is given in Eq. (60). This suggests the natural choice

$$\boldsymbol{\Omega}_Q^{(n)} = \Omega_Q^{(n)} \hat{\mathbf{e}}_z, \quad (61)$$

where  $\hat{\mathbf{e}}_z = [0, 0, 1]$  is a unit vector along the  $z$ -axis. Indeed, on using Eqs. (4) and (5), a simple calculation yields

$$\hat{\mathbf{e}}_z \times \mathbf{t} = (k_0/\alpha) \mathbf{n} ; \quad \hat{\mathbf{e}}_z \times \mathbf{b} = -(\tau_0/\alpha) \mathbf{n}, \quad (62)$$

where  $\alpha = \sqrt{(k_0^2 + \tau_0^2)}$ . On using Eqs. (61) and (60), along with Eq. (62), a short calculation shows that the RHS of Eq. (59) becomes

$$\boldsymbol{\Omega}_Q^{(n)} \times \hat{\mathbf{T}}^{(n)}(s, \xi) = \frac{\Omega_Q^{(n)}}{E^{(n)}(\xi) \sqrt{(k_0^2 + \tau_0^2)}} [k_0 + (k_0^2 + \tau_0^2)\xi] \mathbf{n}. \quad (63)$$

Since  $\hat{\boldsymbol{\xi}}$  is along the normal  $\mathbf{n}$ , substituting Eq. (63) in Eq. (59), and using  $(dE^{(n)}/d\xi) = 2[k_0 + (k_0^2 + \tau_0^2)\xi]$  [from Eq. (14)] on its LHS, a short calculation yields

$$\Omega_Q^{(n)}(k, \xi) = \frac{\hbar}{2mk} \sqrt{(k_0^2 + \tau_0^2)} E^{(n)}(\xi) G^{(n)}(k, \xi). \quad (64)$$

Using the above expression, the angular velocity vector for the normal ribbon is given by  $\boldsymbol{\Omega}_Q^{(n)} = \Omega_Q^{(n)}(k, \xi) \hat{\mathbf{e}}_z$ , as seen from Eq. (61). Hence its axis is fixed along the  $z$ -axis.

**Binormal helical ribbon:** Here, proceeding as in the case of the normal ribbon, using Eq. (8) in Eq. (51) yields

$$\hat{\mathbf{T}}^{(b)}(s, \xi) = \frac{\mathbf{X}_s^{(b)}}{|\mathbf{X}_s^{(b)}|} = (\mathbf{t} - \tau_0\xi\mathbf{n})/E^{(b)}(\xi). \quad (65)$$

Since  $\hat{\xi} = \mathbf{b}$  for the binormal ribbon, the LHS of Eq. (59) is a vector along  $\mathbf{b}$ , suggesting the natural choice

$$\Omega_Q^{(b)} = -\Omega_Q^{(b)} \mathbf{n}. \quad (66)$$

From Eq. (5), we find that  $\mathbf{n}$  is a unit vector in the  $(x, y)$  plane. On using Eqs. (66) and (65), the RHS of Eq. (59) yields

$$\Omega_Q^{(b)} \times \hat{\mathbf{T}}^{(b)}(s, \xi) = [\Omega_Q^{(b)}/E^{(b)}(\xi)] \mathbf{b}. \quad (67)$$

Since  $\hat{\xi}$  is along the binormal  $\mathbf{b}$ , substituting  $(dE^{(b)}/d\xi) = 2\tau_0^2\xi$  [from Eq. (15)] on the LHS of Eq. (59) and simplifying, we find

$$\Omega_Q^{(b)}(k, \xi) = \frac{\hbar}{2mk} \tau_0^2 E^{(b)}(\xi) G^{(b)}(k, \xi) \xi. \quad (68)$$

Using the above expression, the angular velocity vector for the binormal ribbon is given by  $\Omega_Q^{(b)} = \Omega_Q^{(b)}(k, \xi) \mathbf{n}$ , as seen from Eq. (66). This shows that the axis of the angular velocity  $\Omega_Q^{(b)}$  of the rotating frame for the binormal ribbon is itself rotating in the  $(x, y)$  plane, indicating precession. The physical interpretation for the appearance of the linear term  $\xi$  in Eq. (68) will be given in the next section.

We consider ribbons of length  $L(q)$  composed of integer  $q$  turns. As we have shown in Eq. (32),  $k$  takes on *quantized* nonzero values  $k = k_{n,q} = (n/2q)\sqrt{(k_0^2 + \tau_0^2)}$ ,  $n = 1, 2, 3, \dots, q$ , with  $q = 1, 2, 3, \dots$ . Note that in Eqs. (64) and (68), the expressions for  $G^{(n)}(k, \xi)$  and  $G^{(b)}(k, \xi)$  are obtained by setting  $E(\xi) = E^{(n)}(\xi)$  and  $E(\xi) = E^{(b)}(\xi)$  respectively, in Eq. (56), and substituting the quantized values of  $k$  in them. Simplifying, Eq. (64) yields

$$\Omega_Q^{(n)}(n, q, \xi) = \frac{\hbar}{m} \frac{q}{n} \frac{\left[ (k_0^2 + \tau_0^2) \left( 1 - \frac{n^2}{q^2} \right) E^{(n)}(\xi) + 2\tau_0^2 \right]}{[E^{(n)}(\xi)]^2} \quad (69)$$

for the normal ribbon. Likewise, Eq. (68) gives

$$\Omega_Q^{(b)}(n, q, \xi) = \frac{\hbar}{m} \frac{q}{n} \frac{\tau_0^2}{\sqrt{(k_0^2 + \tau_0^2)}} \frac{[(k_0^2 + \tau_0^2)(1 - \frac{n^2}{q^2})E^{(b)}(\xi) + 2\tau_0^2]}{[E^{(b)}(\xi)]^2} \xi \quad (70)$$

for the binormal ribbon.

Note that  $k_0$  and  $\tau_0$  are nonzero constants, and  $n$  is nonzero. Hence the quantum analogs of the angular velocities we have found in Eqs. (69) and (70) are well-defined quantities.

Specializing to *long ribbons* with number of turns  $q \gg 1$  the angular velocity for the low momenta localized states with  $n \ll q$ , the term  $(1 - \frac{n^2}{q^2})$  goes to unity. Hence for both the ribbons, the angular

velocity becomes proportional to  $\frac{q}{n}$  in this case. Therefore as  $n$  increases, the quantum effect gets less pronounced, as expected physically.

### 5.3 Comparison of rotating frame angular velocities obtained for normal and binormal helical ribbons

It is instructive to present the physical interpretation of the expressions for the quantum analog of the Coriolis rotating frame angular velocities obtained for the normal and binormal helical ribbons, respectively, and compare them.

Firstly, the appearance of  $\hbar$  in the general expressions for the angular velocity of the frame of rotation for the normal helical ribbon  $\Omega_Q^{(n)}(k, \xi)$  and binormal helical ribbon  $\Omega_Q^{(b)}(k, \xi)$ , given in Eqs. (64) and (68) respectively, shows that they are indeed quantum analogs.

On a helical ribbon, for every width point  $\xi$ , there is a helix, and a quantum particle moving on the helix with a momentum  $k$  experiences a push that depends on  $\xi$ . Hence the quantum analog of the angular velocity of the rotating frame that causes the Coriolis effect depends on  $k$  and  $\xi$ , as expected.

The dependence of the angular velocities on the width coordinate  $\xi$  is *distinct* for the two ribbons, as seen from the general expressions given in Eqs. (64) and (68). This can be understood as follows. Note that in  $\Omega_Q^{(b)}(k, \xi)$ , the linear dependence on  $\xi$  implies that the force on the particle on a binormal ribbon acts in opposite directions for  $\xi < 0$  and  $\xi > 0$ . This leads to quantum localization at the central helix on the binormal helical ribbon as required. This is unlike for the normal ribbon where  $\Omega_Q^{(n)}(k, \xi)$  does not change its sign as  $\xi$  changes sign, since  $E^{(n)}(\xi)$  is positive for both signs of  $\xi$ , as seen from Eq. (14). This results in localization near the inner edge of the normal ribbon as needed. Thus, the expressions of the angular velocities obtained are consistent with our results on quantum localization.

The angular velocity of the rotating frame in the Coriolis effect is taken to be a constant in most books on classical mechanics [20]. However, the quantum expressions in Eqs. (64) and (68) are dependent on the wave vector  $k$ , which essentially translates to the velocity of the particle in the classical scenario. Such a dependence is not unphysical. For example, angular velocities of rotation in some fluids depend on the particle flow velocity [26]. Such dependencies can also appear if the underlying dynamics of the physical

system considered is nonlinear [27].

Note that the derivation of the angular velocity of the Coriolis rotating frame for a helical ribbon uses the Frenet-Serret equations, which in turn represent the rotating frame of the Frenet triad, as explained below Eq. (1). This shows an implicit connection between these two rotating frames.

In summary, *given* the quantum geometric potential that is the cause of the localization of a moving particle on the width of the ribbon, suggesting the presence of a pseudo-force, our aim was to *find* a consistent quantum analog of the angular velocity  $\mathbf{\Omega}$  for the rotating frame on the ribbon in such a way that this phenomenon can be interpreted as the quantum analog of the Coriolis effect. We have achieved that.

## 6 Discussion

Most of the results obtained in this paper have been summarized in the Introduction. It is important to note that geometric effects on quantum particle transport (induced by the curvature and torsion of helical ribbons) which we have studied in this paper are much deeper and much more general than this particular example, with its roots in the concept of parallel transport of a vector around a closed path on a curved manifold and the associated anholonomy. This leads [28] to the appearance of a Berry connection as well as a Berry curvature, representing the analogous vector potential and its corresponding divergence-free ‘magnetic field’, respectively. In addition, the integral of the Berry connection leads to a Berry phase for the wave function. These have appeared in diverse contexts in physics [29].

Parallel transport of a vector on a curved surface was analyzed over three decades ago [30], by regarding the surface as an evolving space curve. By using the Darboux rotation of the Frenet-frame, a general expression for the anholonomy that arises for a closed path on the curved surface was derived, with the emergence of a vector potential and a geometric phase. Non-commutative geometry is inherent in the quantum phenomena that arise in systems associated with a vector potential. Recently, topological invariants and their underlying geometric structure have been considered in general [31]. We plan to apply these results to helical ribbons in a separate paper.

Our continuum analysis is valid in the ballistic regime, which is accessible in experiments on nanorib-

bons [32]. The methodology we have presented for helical ribbons can also be extended to other curved surfaces. Diverse devices that are applications of the effect of geometry on quantum transport, controlled by appropriately tuning the curved surface geometry of the surface considered, can be envisaged in nanotechnology and biotechnology. As our results show, the interplay between quantum mechanics and curved geometry can be experienced not only by electrons, where it manifests itself as a Hall-like effect on helical ribbons, but by other quantum particles as well, under suitable scenarios.

Quantum mechanics of particles on curved manifolds can lead to new phenomena. As mentioned in the Introduction, it has recently been noted [19] that in the case of a three dimensional spirally stacked tungsten disulfide ( $\text{WS}_2$ ), “the twisting structure and the Coriolis-like force were guiding the electrons”, leading to a ‘twistronic Hall effect’ [18]. This system is different from the helical ribbons we have studied in the present paper. We hope that our work will motivate experiments to study transport of quantum particles on normal and binormal helical nanoribbons to look for novel effects.

## 7 Acknowledgments

The work of A.S. at Los Alamos National Laboratory was carried out under the auspices of the U.S. DOE and NNSA under Contract No. 89233218CNA000001.

## References

- [1] J. D. Watson and F. H. C. Crick, *Nature* **171**, 737 (1953).
- [2] L. Pauling and R. B. Corey, *Proc. Nat. Acad. Sci. (USA)* **37**, 729 (1951); *ibid* L. Pauling, R. B. Corey, and H. R. Branson **37**, 205 (1951); *ibid* **39**, 84 (1953).
- [3] D. J. Bell, Y. Sun, L. Zhang, L. X. Dong, B. J. Nelson, and D. Grützmacher, *Sensors and Actuators A* **130-131**, 54 (2006).
- [4] M. Tounsi *et al.*, *Electroanalysis* **28**, 2892 (2016); V. M. Freixas *et al.*, *J. Am. Chem. Soc.* **145**, 21012 (2023).



- [5] P. X. Gao *et al.*, Science **309**, 1700 (2005).
- [6] For reviews on fabrication of nanohelices, see L. Liu *et al.* Nanoscale **6**, 9355 (2014); Z. Ren and P. X. Gao, Nanoscale **6**, 9366 (2014).
- [7] L. Prevost *et al.*, ACS Nano **16**, 10581 (2022).
- [8] X. Fan *et al.*, Nano Lett. **20**, 2667 (2020) and references therein.
- [9] A. Goriely and P. Shipman, Phys. Rev. E, **61**, 4508 (2000) and references therein.
- [10] A. F. Fonseca, C. P. Malta, and D. S. Galvao, Nanotechnology **18**, 435606 (2007).
- [11] H. Zhan *et al.*, Nanoscale **10**, 18961 (2018).
- [12] R. C. T. da Costa, Phys. Rev. A **23**, 1982 (1981).
- [13] D. J. Struik, *Lectures on Classical Differential Geometry* (2nd ed. Dover, Reading, MA, 1988); L. P. Eisenhart, *A treatise on the Differential Geometry of Curves and Surfaces* (Dover, New York, 1960); A. Pressley, *Elementary Differential Geometry* (Springer SUMS 2010).
- [14] C. Kittel, *Introduction to Solid State Physics* (John Wiley and Sons, Inc., 8th Edition 2005).
- [15] D. Yoshioka, The Quantum Hall Effect (Springer Series in Solid-State Sciences, Springer-Verlag, Berlin, 2002).
- [16] N. Nagaosa, J. Sinova, S. Onoda, A. H. MacDonald, and N. P. Ong, Rev. Mod. Phys. **82**, 1539 (2010).
- [17] C.-Z. Chang, C.-X. Liu, and A. H. MacDonald, Rev. Mod. Phys. **95**, 011002 (2023).
- [18] Zhurun Ji *et al.*, Nature **634**, 69 (2024).
- [19] <https://phys.org/news/2024-10-theoretical-physicist-uncovers-layers-material.html>;  
<https://penntoday.upenn.edu/news/idea-rooted-twistronics-yields-electrifying-dizzying-outcome>
- [20] See, for e.g., H. Goldstein, C. P. Poole, and J. L. Safco, *Classical Mechanics* (Pearson Education Inc., 3rd Edition, 2002).

- [21] B. Gardas, S. Deffner, and A. Saxena, Phys. Rev. A **94**, 022121 (2016).
- [22] A. Messiah, *Quantum Mechanics* Vol I, (North Holland Publishing Company, Amsterdam (1961))
- [23] J. D. M. de Lima *et al.*, Eur. Phys. J. Plus **136**, 551 (2021).
- [24] In the context of twisted surfaces, a helicoidal strip was the first example where a metric induced effective potential which is purely quantum mechanical in origin was found. Its connection with a Hall-like effect was also noted. See R. Dandoloff and T. T. Truong, Phys. Lett. A **325**, 233 (2004).
- [25] Further extensions of reference [24] may be found in V. Atanasov and R. Dandoloff, Phys. Lett. A **371**, 118 (2007); V. Atanasov, R. Dandoloff, and A. Saxena, Phys. Rev. B **79**, 033404 (2009); V. Atanasov and A. Saxena, Phys. Rev. B **81**, 205409 (2010); Phys. Rev. B **92**, 035440 (2015).
- [26] J. W. M. Bush, H. A. Stone, and J. P. Tazosh, Current Topics in the Phys. of Fluids **1**, 337 (1994).
- [27] S. H. Strogatz, *Nonlinear Dynamics and Chaos*, Third ed. (CRC Press, Boca Raton, FL, 2024).
- [28] M. V. Berry, Proc. R. Soc. Lond. Ser. A **392**, 45 (1984).
- [29] See, for e.g., A. Shapere, F. Wilczek (Eds.), *Geometrical Phases in Physics* (World Scientific, Singapore, 1989).
- [30] R. Balakrishnan, A. R. Bishop, and R. Dandoloff, Phys. Rev. Lett. **64**, 2107 (1990); Phys. Rev. B **47**, 3108 (1993).
- [31] R. Balakrishnan, R. Dandoloff, and A. Saxena, Phys. Lett. A **493**, 129261(2024).
- [32] J. Baringhaus *et al.*, Nature **506**, 7488 (2014).